



Genesis and mineralogical studies of zircons in the Alamas, Yurungkash and Karakash Rivers nephrite deposits, Western Kunlun, Xinjiang, China



Yuntao Jing ^{a,b}, Yan Liu ^{a,b,*}

^a Southern Marine Science and Engineering Guangdong Laboratory (Guangzhou), Guangzhou 511458, PR China

^b Key Laboratory of Deep-Earth Dynamics, Institute of Geology, Chinese Academy of Geological Sciences, Beijing 100037, PR China

ARTICLE INFO

Keywords:

Mg-skarn
Nephrite
Baddeleyite
Igneous zircon
High $\delta^{18}\text{O}$
Xinjiang

ABSTRACT

Nephrite, an aggregate of fine-grained tremolite or actinolite, is mainly found in Mg-skarn at the contact zone between granitoids and dolomitic marble. The nephrite belt in the southern Western Kunlun Mountains in China is the largest in the world, and includes 11 major skarn deposits and >20 orebodies including the Alamas deposit. In addition, economic placer nephrite deposits occur along the Yurungkash & Karakash Rivers. The nephrite in these deposits contains numerous zircons and some grains have high $\delta^{18}\text{O}$ values, but the genesis of these zircons is not clear. In this study, we investigated the formation mechanism of the nephrite and origin of zircons in nephrite based on the geochemical and $\delta^{18}\text{O}$ characteristics of zircons in nephrite from the deposits at Alamas and along the Yurungkash & Karakash Rivers, as well as the C—O isotopes of the dolomitic marble at Alamas. We found that zircons in nephrite often occur with tremolite and apatite and the major elements of these zircons are close to those of common magmatic zircon. Zircon grains in the Alamas nephrite are mainly subhedral, 80–130 μm long, 50–90 μm wide, and have clear oscillatory zoning. These zircons have similar REE patterns with Alamas granodiorite, including heavy REE (HREE) enrichment and large positive Ce anomalies ($\text{Ce}/\text{Ce}^* = 5.30\text{--}368$). Such petrographic and geochemical characteristics suggest most zircons are magmatic zircons, with some experienced hydrothermal alteration. Zircon $\delta^{18}\text{O}$ values in Alamas nephrite are 5.69 ‰–8.85 ‰ ($n = 25$; an exception of 13.35 ‰), close to those zircons in Alamas granodiorite (6.4 ‰–9.0 ‰) but higher than mantle magmatic zircon (5.3 ± 0.3 ‰). The $\delta^{13}\text{C}$ (0.79 ‰–1.02 ‰) and $\delta^{18}\text{O}$ (18.7 ‰–20.6 ‰) values of the Alamas dolomitic marble indicate formation by the partial dissolution of marine carbonate rocks. Zircons in nephrite from Yurungkash & Karakash Rivers deposits are mainly subhedral, 100–160 μm long, 80–30 μm wide, and show clear or obscure irregular zoning. They show HREE enrichment and relatively weak positive Ce anomalies (2.58–35.8), suggesting most zircons have magmatic origin, with some experienced hydrothermal alteration. Zircons from Yurungkash & Karakash Rivers have $\delta^{18}\text{O}$ values range from 14.6 ‰ to 21.37 ‰ ($n = 31$; an exception of 9.03 ‰). Irregular baddeleyite grains occur in the nephrite, and fragmented or granular grains occur locally within the nephrite zircons or fissures of zircon. These baddeleyite may have formed via the following reaction between zircon and dolomite: $2\text{ZrSiO}_4 + \text{CaMg}[\text{CO}_3]_2 \rightarrow 2\text{ZrO}_2 + \text{CaMg}[\text{SiO}_3]_2 + 2\text{CO}_2$ at 660–710 °C and 3 kbar. In Yurungkash & Karakash Rivers nephrite deposits, considering these placer nephrite come from Mg-skarn, these high $\delta^{18}\text{O}$ zircons probably have initially formed within endoskarn, close to the margin of the granitoid where marble with high $\delta^{18}\text{O}$ was assimilated into the melt, and retain nice oscillatory and/or sector zoning.

1. Introduction

Skarns typically exhibit a temporal evolution from high-temperature phases precipitated from magmatic fluids to marble and hornfels resulting from isochemical thermal metamorphism and finally low-temperature assemblages related to meteoric and basinal fluids

(Einaudi et al., 1981; Meinert et al., 2005; Rubenach, 2013). This type of Mg-skarn hosts important non-metallic deposits, including nephrite. Such nephrite deposits form as a result of metasomatic or metamorphic processes (Leaming, 1978; Harlow and Sorensen, 2001, 2005) and commonly record a magmatic stage, a contact metamorphic stage, and prograde and retrograde metasomatic stages, with each stage giving rise

* Corresponding author.

E-mail address: ly@cags.ac.cn (Y. Liu).

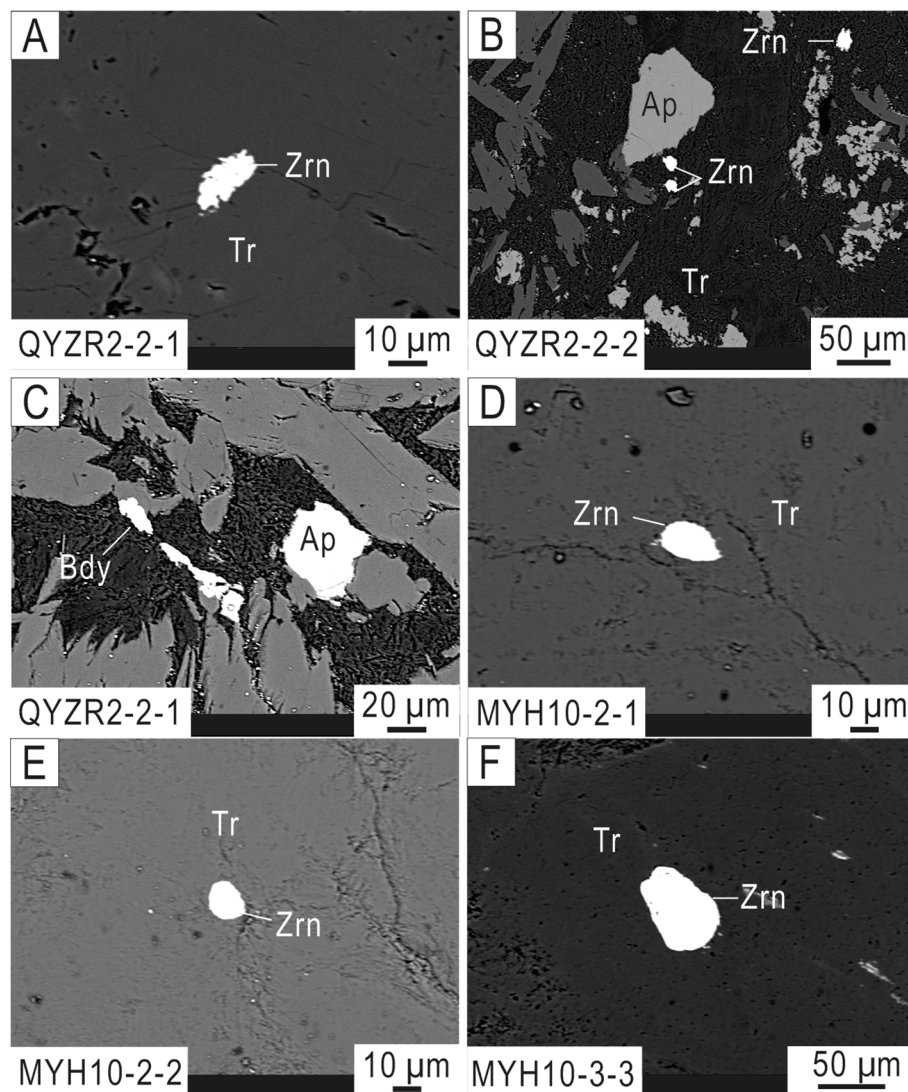


Fig. 1. Backscattered electron (BSE) images of zircon (Zrn) and baddeleyite (Bdy) in samples from the (A–C) Alamas deposit (sample QYZR2) and (D–F) Yurungkash & Karakash Rivers deposits (MYH10).

to a distinct mineral assemblage in the contact zone (Liu et al., 2011, 2015). Dolomite-related nephrite deposits are thought to reflect contact metasomatic processes driven by magmatic fluids (Harlow and Sorensen, 2001; Yui and Kwon, 2002).

Nephrite deposits mainly occur in Mg-skarns in the Western Kunlun of Xinjiang, China. It is thought that the Hetian nephrite deposits in this region, including the Alamas deposit, formed through contact metasomatism of Mg-carbonates by local granitoid intrusions (Tang et al., 1994; Liu et al., 2010, 2011). Previous studies of the Alamas granodiorites, Alamas and Yurungkash & Karakash Rivers nephrite have reported the geological setting, nephrite mineralogy and geochemistry, and zircon petrography, U–Pb ages and trace element compositions (Liu et al., 2015, 2016; Zhang et al., 2016). The formation of nephrite is thought to have been influenced by multi-stage tectonic events and fluid activities, with coarse-grained tremolite being replaced by fine-grained tremolite. Three possible fluid sources have been suggested: meteoric water, magmatic water, and CO₂ derived from the decarbonation of dolomite (Liu et al., 2011). Zircon grains in the Alamas granodiorite are mainly euhedral, prismatic, colorless, with typical igneous oscillatory zoning, U–Pb ages and contain small inclusions of albite, biotite, and feldspar, suggesting a magmatic origin (Zhang et al., 2016). Similarities in morphologies, geochemical signatures, U–Pb ages and contain a few mineral inclusions indicate that most zircons in the nephrite from

Hetian-Yutian have magmatic origin and were derived from the granodiorite (Liu et al., 2015, 2016).

Zircon is a common accessory mineral in sedimentary, magmatic, and metamorphic rocks. It has a particularly stable structure and can record information on the magmatic rocks in which it originally crystallized (Valley et al., 1994, 2005; Cavosie et al., 2011; Spencer et al., 2017). Zircon δ¹⁸O analysis can distinguish magmas derived directly from the mantle or from those that affected by supracrustal materials into melts, which commonly have higher δ¹⁸O values, and can thus effectively reveal crust–mantle interactions (Bindeman and Valley, 2000, 2001; Monani and Valley, 2001; Peck et al., 2001; Wei et al., 2008; Grimes et al., 2013). The mantle is a remarkably homogeneous oxygen isotope reservoir (Eiler, 2001). On average, igneous zircons in high-temperature equilibrium with mantle magmas have δ¹⁸O values of 5.3 ‰ ± 0.3 ‰ (Valley et al., 1998). Globally, 99.3 % of igneous zircons have δ¹⁸O values of <13.8 ‰; moreover, the δ¹⁸O values show an obvious change after the Paleoproterozoic–Neoarchean boundary (2500 Ma; Spencer et al., 2022). However, magma that results from the melting of high-δ¹⁸O materials (e.g., pelitic sediments) can crystallize extremely high-δ¹⁸O zircons (>15 ‰; Spencer et al., 2017). Given that sediments (δ¹⁸O = 15 ‰–25 ‰) are the dominant reservoir of high-δ¹⁸O material on earth, any process that changes sediment δ¹⁸O or the quantity of sediments available for melting will effect the δ¹⁸O values of

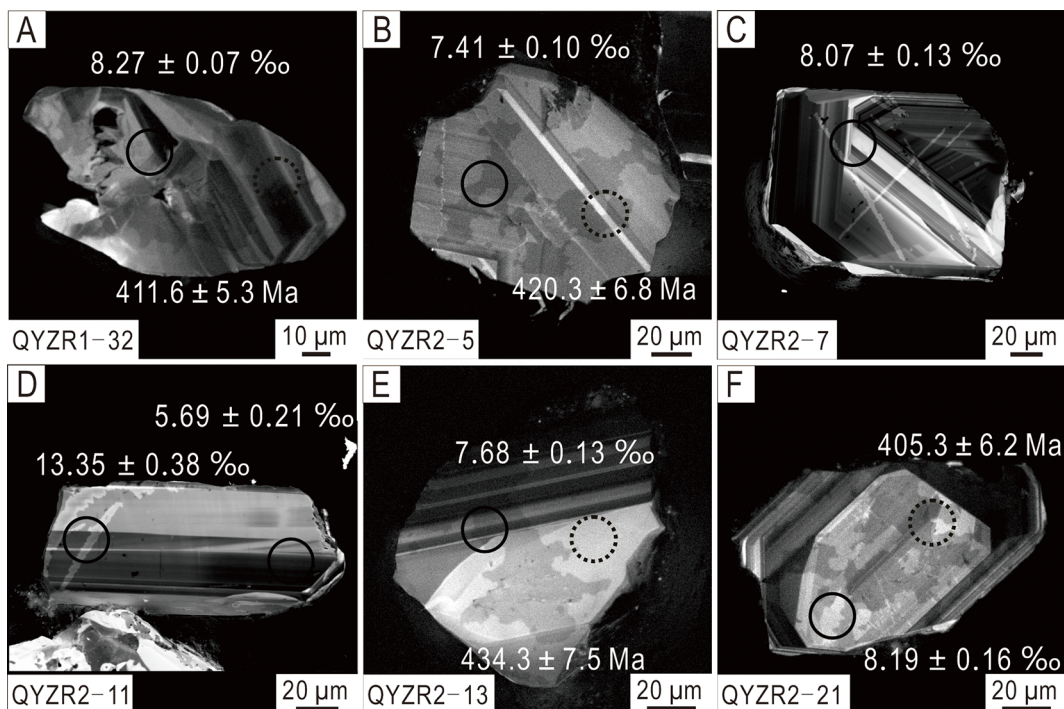


Fig. 2. Cathodoluminescence images of zircons from Alamas nephrite deposit, showing SHRIMP U–Pb ages (dotted circles, data from Liu et al., 2015) and oxygen isotope data (solid circles); numbers correspond to the analytical data presented in Table 4.

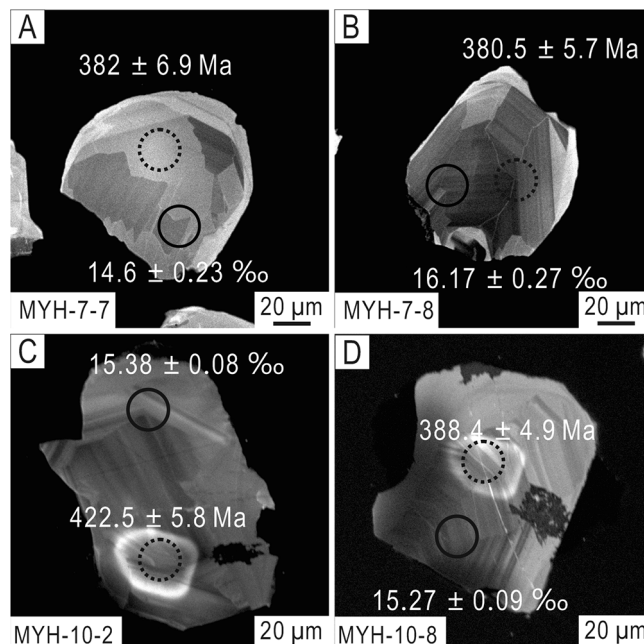


Fig. 3. Cathodoluminescence images of zircons from Yurungkash & Karakash Rivers placer nephrite deposits (samples MYH7, MYH10, and MYH20), showing SHRIMP U–Pb ages (dotted circles, data from Liu et al., 2016) and oxygen isotope data (solid circles); numbers correspond to the analytical data presented in Table 4.

igneous rocks and their zircons (Taylor, 1968; Valley et al., 2005). In addition, high- $\delta^{18}\text{O}$ zircons can crystallize in metamorphic marble, in which the dissolution of detrital zircons provide Zr for metamorphic zircons and baddeleyite. Such zircons can be affected by dissolution and reprecipitation, which can modify or obscure the original zoning (Claesson et al., 2016; Roberts and Santosh, 2018). Disequilibrium between whole-rock and zircon $\delta^{18}\text{O}$ isotope values is most likely caused by metamorphic devolatilization or interaction with an H₂O-dominant fluid sourced from the host rocks (Zheng et al., 1998).

The origin and occurrence of the Hetian nephrite ore belt have been studied in detail (Liu et al., 2015, 2016). In this study, we constrain the genesis of zircons in nephrite, based on the geological, petrographical, geochemical, and isotopic characteristics of zircons in samples from the Alamas and Yurungkash & Karakash Rivers deposits, and C–O isotopes value of the Alamas dolomitic marble. We found that $\delta^{18}\text{O}$ values of zircons in nephrite vary markedly (5.69 ‰ to 21.37 ‰), and sometimes greatly exceed the values of zircons in the Alamas granodiorite ($\delta^{18}\text{O} = 6.4\text{ ‰–}9.0\text{ ‰}$). The reasons for the variation in zircon $\delta^{18}\text{O}$ values and

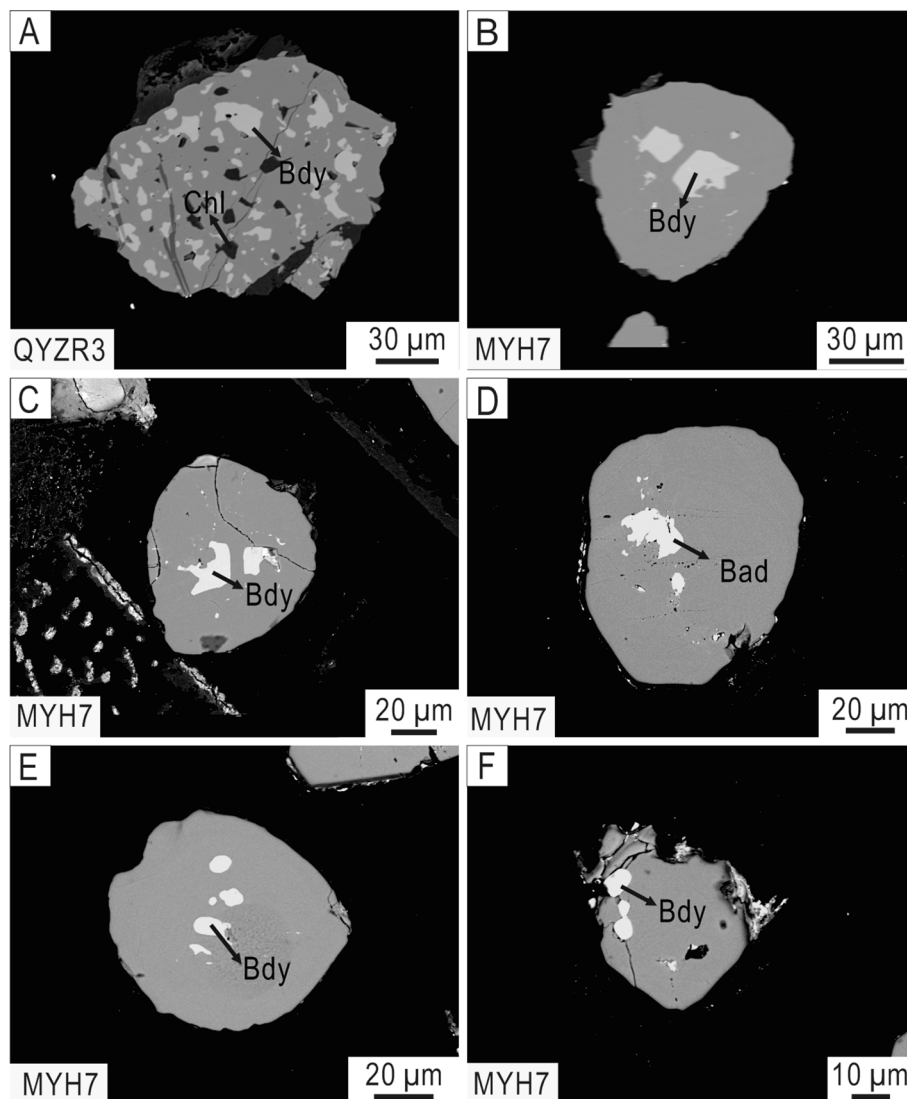


Fig. 4. Backscattered electron (BSE) images of zircon inclusions in samples from the (A) Alamas and (B–F) Yurungkash & Karakash Rivers nephrite deposits. (A) Baddeleyite (Bdy) and chlorite (Chl) grains in zircon. (B–F) Fragmentary or granular baddeleyite distributed in the interior or fissures of zircon.

the genesis of such zicons in the Mg-skarn were discussed in detail.

2. Geological setting

Geologically, Xinjiang can be divided into the Northern Xinjiang and Southern Xinjiang separated by the Tianshan Mountains. North Xinjiang is an important ore belt in China, which is characterized by metal deposits. In contrast, Southern Xinjiang is famous for its nonmetal deposits (Mao et al., 2005), such as nephrite and asbestos in the Kunlun Mountains (Liu et al., 2015).

The Kunlun Mountains are divided into the Western and Eastern Kunlun mountains by longitude 81°E. Most nephrite deposits are found in the Western Kunlun Orogen (WKO), which is a 1000 km long early Paleozoic orogenic belt located along the northern periphery of the Tibetan Plateau, bordering the Pamir in the west and the Altyn-East Kunlun Orogen in the east. The WKO is of great significance for understanding the reconstruction of paleo-Asia Block, because it occupies a key tectonic position between the Tarim Block to the north and the Tethyan domain to the south (Deng et al., 2013, 2014; Gao and Reiner, 2000; Wang et al., 2001; Xiao et al., 2001, 2005; Yang et al., 2007).

The giant nephrite belt is located in the south of the WKO, Xinjiang, China, and consists of three main primary nephrite ore belt as

Shache-Yecheng, Hetian-Yutian, and Qiemo-Ruoqiang. Most nephrite deposits occur in similar geological settings, and most of them are located at the contact zone between Precambrian dolomitic marbles and intermediate-acidic igneous rocks. Placer nephrite deposits are found within the terraces of the Yurungkash (White Jade) and Karakash (Black Jade) Rivers in the Hetian area (Jiang, 1986; Liu et al., 2011, 2015, 2016).

2.1. Alamas nephrite deposit

Alamas deposit is located 65 km southeast of Liushen village in Yutian County ($N36^{\circ}12'$, $E81^{\circ}55'$), at an elevation of about 4500 m. Granite and granodiorite are more widely distributed than diorite and quartz diorite around the nephrite orebodies in No. 11 nephrite vein of Alamas nephrite deposit. The Alamas granitic rocks are I-type granite formed through partial melting of mafic lower crust with a component of mantle-derived magma, and records the fractional crystallization of hornblende, biotite, and accessory apatite, allanite, and Fe-Ti oxides (Zhang et al., 2016). Zircons in Alamas granite yield a concordia age of 445.6 ± 2.5 Ma, corresponding to the post-collision stage of the Proto-Tethys ocean basin (Zhang et al., 2016). The wallrock for the Alamas nephrite deposit is Precambrian dolomitic marble. Mineral zonings, with

Table 1
Electron microprobe data of zircon major and trace element contents (wt.%) in nephrite from Alamas and Yurungkash & Karakashgar Rivers deposits of Xinjiang, China.

Alamas deposit Samples	F	Na ₂ O	Al ₂ O ₃	MgO	K ₂ O	CaO	P ₂ O ₅	TiO ₂	MnO	HfO ₂	ZrO ₂	SiO ₂	Cl	FeO	UO ₂	ThO ₂	Total	Zn/Hf	Th/U
QYZR-1-2-1	0.00	0.02	0.00	0.00	0.00	0.02	0.00	0.00	0.04	1.18	61.94	34.82	0.00	0.02	0.59	0.08	98.70	52.62	0.14
QYZR-1-2-2	0.19	0.03	0.00	0.00	0.00	0.02	0.00	0.01	0.00	1.39	63.24	35.58	0.00	0.03	0.50	0.00	100.49	45.46	0.00
QYZR-1-3-1	0.00	0.02	0.00	0.02	0.00	0.03	0.00	0.02	0.03	0.62	63.39	34.57	0.00	0.01	0.51	0.11	99.33	101.91	0.21
QYZR-1-21-1	0.08	0.00	0.01	0.01	0.00	0.00	0.00	0.00	0.00	0.76	62.94	34.65	0.00	0.00	0.02	0.00	98.49	83.14	0.00
QYZR-1-21-2	0.08	0.00	0.00	0.03	0.00	0.00	0.00	0.00	0.13	0.02	63.30	33.85	0.00	0.00	0.04	0.01	98.11	99.06	0.26
QYZR-3-2-2	0.10	0.03	0.02	0.02	0.00	0.00	0.00	0.00	0.08	0.89	64.42	33.84	0.00	0.05	0.05	0.00	99.48	72.71	0.00
QYZR-3-2-3	0.11	0.02	0.00	0.01	0.00	0.00	0.02	0.00	0.00	0.81	64.76	33.12	0.01	0.00	0.03	0.03	99.00	79.66	0.88
Yurungkash and Karakashgar Rivers deposit																			
MYH-7-3-1	0.01	0.01	0.00	0.00	0.02	0.00	0.05	0.00	0.00	1.32	63.95	34.35	0.00	0.05	0.00	0.00	99.77	48.55	0.00
MYH-7-3-2	0.00	0.01	0.00	0.01	0.00	0.01	0.00	0.05	0.06	1.47	63.58	34.38	0.00	0.05	0.00	0.00	99.62	43.19	0.00
MYH-7-13-1	0.00	0.03	0.00	0.02	0.02	0.00	0.00	0.00	0.08	1.08	63.67	34.80	0.00	0.00	0.04	0.03	99.77	58.79	0.60
MYH-7-13-2	0.00	0.02	0.00	0.01	0.00	0.01	0.00	0.12	0.00	1.08	64.63	34.73	0.01	0.05	0.01	0.04	100.71	60.01	3.67
MYH-7-15-1	0.07	0.00	0.02	0.00	0.00	0.00	0.00	0.00	0.05	1.19	63.74	34.58	0.00	0.01	0.08	0.00	99.74	53.70	0.00
MYH-7-15-2	0.00	0.00	0.00	0.01	0.02	0.00	0.00	0.06	0.02	1.22	63.29	35.10	0.00	0.00	0.11	0.08	99.91	51.83	0.74
MYH-7-15-3	0.04	0.00	0.01	0.01	0.00	0.00	0.00	0.17	0.00	1.15	63.75	34.93	0.00	0.02	0.07	0.05	100.19	55.53	0.79
MYH-10-1-1	0.03	0.02	0.00	0.01	0.01	0.04	0.00	0.03	0.00	1.35	63.14	33.93	0.00	0.00	0.02	0.01	98.59	46.74	0.61
MYH-10-1-2	0.12	0.00	0.01	0.00	0.01	0.02	0.00	0.21	0.05	1.55	63.25	34.39	0.00	0.02	0.00	0.04	99.66	40.94	0.00
MYH-10-1-5	0.13	0.00	0.01	0.01	0.04	0.00	0.00	0.09	0.00	0.41	65.04	34.53	0.00	0.02	0.00	0.00	100.27	159.81	0.00
MYH-10-5-2	0.11	0.02	0.00	0.03	0.00	0.02	0.00	0.00	0.00	1.25	63.35	34.02	0.00	0.00	0.06	0.03	98.89	50.56	0.49
MYH-10-7-1	0.04	0.00	0.00	0.00	0.01	0.00	0.00	0.10	0.04	0.92	63.25	34.65	0.00	0.02	0.03	0.00	99.07	68.60	0.00
MYH-10-7-2	0.00	0.02	0.00	0.00	0.00	0.03	0.00	0.00	0.00	1.06	62.27	34.19	0.00	0.00	0.74	0.03	98.29	59.02	0.04
MYH-10-11-1	0.00	0.02	0.00	0.04	0.01	0.01	0.03	0.18	0.00	1.64	62.49	34.49	0.00	0.03	0.00	0.02	98.97	38.22	0.00
MYH-20-2-2	0.08	0.01	0.02	0.00	0.00	0.00	0.00	0.00	1.08	63.61	33.29	0.00	0.00	0.04	0.03	98.15	58.95	0.68	

diopside (400 °C – 600 °C) close to the granodiorite, and tremolite and serpentine (330 °C – 420 °C) close to the dolomitic marble, indicate a decreasing temperature gradient from granodiorite to marble (Liu et al., 2010, 2011). About 11 nephrite veins have been found in Alamas, with the length up to 20 m (10 m on average) and the width of about 0.1 – 0.5 m. Most veins are distributed along faults and fractures within the dolomitic marble and formed through the metasomatism (Liu et al., 2015).

The widths of the white, white-green, and green zones of nephrite vary from 30 to 50 cm, the narrowest part of the white nephrite belt is 30 cm wide (Liu et al., 2015). Dolomitic marble (ACa1–8) and zircons separated from green nephrite (QYZr1–3) samples in Alamas deposits were selected for C and O isotopes determination.

2.2. Yurungkash and Karakash Rivers nephrite deposit

Placer nephrite in the Yurungkash & Karakash Rivers in Hetian was first discovered in 5000 years ago. Glacial activities and the high altitude of the primary nephrite deposits are the two main factors that led to the formation of the placer nephrite (Liu et al., 2016). Black and green nephrite samples (MYH7, MYH10, MYH20) from Yurungkash & Karakash Rivers deposit (N37°30'8.6", E79°39'2.8"; ~1.3 km above sea level) were selected for zircons separation and $\delta^{18}\text{O}$ studies, respectively.

3. Results

All the analytical methods are described in the supplementary material.

3.1. Petrographic studies of zircons

Nephrite consists predominately of tremolite, with minor diopside, chlorite, epidote, apatite, titanite, zircon, calcite and phlogopite (Liu et al., 2015, 2016). In nephrite samples QYZr2 and MYH10, some nephrite show signs of brittle deformation, with some dendritic fissures (Fig. 1A, D and E), consistent with the several generations of tremolite and local geology. In space, green and black nephrite is closer to granodiorite, while white nephrite is closer to dolomitic marble. Zircons are common and generally occur in green and black nephrite rather than white and green-white nephrite, corresponding to the zonation of skarn. Zircons occur generally closely associated with tremolite and apatite, and they are scattered in nephrite rather than along fissures or a foliation, suggesting that zircons formed earlier than the other minerals. Zircons are irregular or oval in shape, with lengths of 30–60 μm and widths of 10–40 μm (Fig. 1A, B and D–F). In sample QYZR2-2-1, the baddeleyite occurs together with apatite in an irregular intermittent strip shape (Fig. 1C), rather than euhedral, with length of 20 μm and width of 5 μm .

The internal structure and mineral inclusions of zircons from nephrite were observed by CL and BSE images. Zircons separated from Alamas nephrite are mainly subhedral, with lengths of 100 ~ 280 μm and widths of 80 ~ 160 μm (Fig. 2). Most zircons have clear oscillatory zones (Fig. 2A and C), and a few zircons have obscure oscillatory zones (Fig. 2B), indicating that these magmatic zircons may have experienced hydrothermal fluid alteration. Zircon grains separated from Yurungkash & Karakash Rivers nephrite are mainly subhedral, with lengths of 100 ~ 160 μm and widths of 80 ~ 130 μm (Fig. 3). Some of them have obscure irregular zoning (Fig. 3A), and some of them have clear oscillatory zoning (Fig. 3B).

Baddeleyite grains are rare in zircons in nephrite and some accompanied by fissures (Fig. 4). They are scattered, residual or granular, distributed irregularly in zircons or fissures of zircons, with lengths up to 20 μm and widths up to 10 μm .

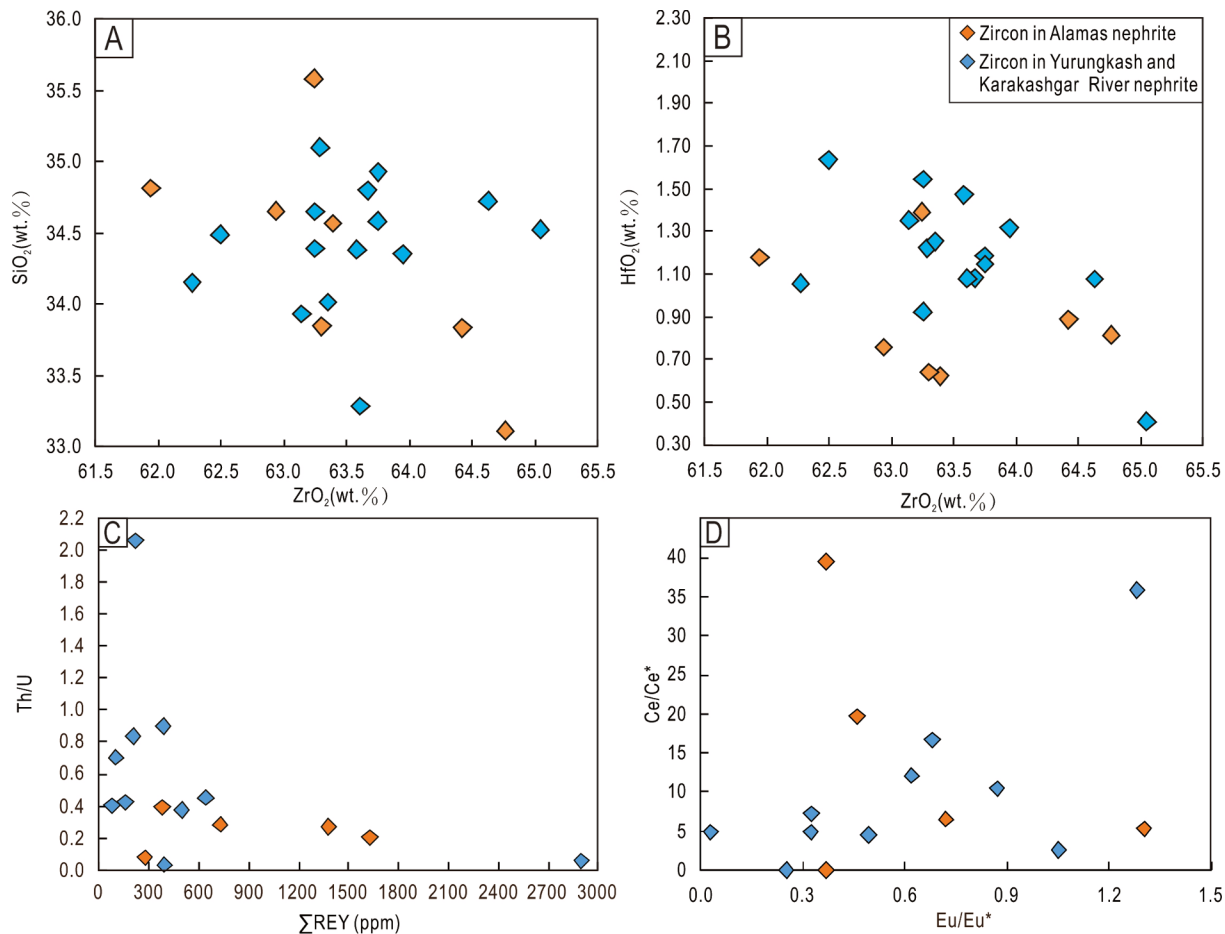


Fig. 5. (A) ZrO₂ vs SiO₂, (B) ZrO₂ vs HfO₂ diagrams by EMPA; and (C) Th/U vs ΣREY, and (D) Ce/Ce* vs Eu/Eu* diagrams by LA-ICP-MS for zircons in nephrite from Alamas and Yurungkash & Karakashgar Rivers deposits of Xinjiang, China. Abbreviations: REY, rare earth elements and yttrium. Eu and Ce anomalies were calculated in this manner: Ce/Ce* = Ce_N/(sqrt(La_N*Pr_N)), Eu/Eu* = Eu_N/(sqrt(Sm_N*Gd_N)).

3.2. Major and trace element of zircons

The EPMA result shows that major elements in zircons from Alamas nephrite (Table 1). The ZrO₂ contents rang from 61.9 to 64.8 % (with an average value of 63.4 %, n = 7), SiO₂ contents from 33.1 to 35.6 % (with an average value of 34.3 %, n = 7), HfO₂ contents from 0.62 to 1.39 % (with an average value of 0.90 %, n = 7). For zircons from Yurungkash & Karakashgar Rivers nephrite, the ZrO₂ contents rang from 62.3 to 65.0 % (with an average value of 63.5 %, n = 15), SiO₂ contents from 33.3 to 35.1 % (with an average value of 34.4 %, n = 15), HfO₂ contents from 0.41 to 1.64 % (with an average value of 1.18 %, n = 15). Compared with the main element oxides in the standard chemical formula of zircon (ZrO₂ = 67.2 %, SiO₂ = 32.8 %, HfO₂ = 0.5 ~ 2.0 %, (Hoskin, 2003)), zircons in nephrite have lower ZrO₂ contents and higher SiO₂ contents, and also contain a small amount of trace elements such as Hf, U, Th, Ti. The ZrO₂, SiO₂ and HfO₂ contents (Fig. 5A and B). And there are no significant difference in zircons among Alamas and Yurungkash & Karakashgar Rivers nephrite.

The LA-ICP-MS result shows that trace elements in zircons from Alamas nephrite. The Th/U ratios range from 0.08 to 0.39 (with an average value of 0.27), Ce/Ce* ratios from 5.30 to 368 (with an average value of 84.2), Eu/Eu* ratios from 0.37 to 1.30 (with an average value of 0.58), ΣREY contents from 276 to 12949 ppm (with an average value of 3229 ppm) (Table 2). For zircons from Yurungkash & Karakashgar Rivers nephrite, the Th/U ratios range from 0.03 to 2.06 (with an average value of 0.62), Ce/Ce* ratios from 2.58 to 35.8 (with an average value of 9.9), Eu/Eu* ratios from 0.03 to 1.28 (with an average value of 0.59), ΣREY contents from 77 to 2898 ppm (with an average value of 557 ppm)

(Table 2, Fig. 5 C and D). The REE patterns of zircons in Alamas granodiorite, Alamas and Yurungkash & Karakash Rivers nephrite are similar (Fig. 6). The La- (Sm/La)_N and Sm_N/La_N-Ce/Ce* projections show that most zircons fall in magmatic zircons and some transition to hydrothermal zircons (Fig. 7).

3.3. C-O isotopes of dolomitic marble

The C—O isotope compositions are δ¹³C = 0.79–1.02 ‰, δ¹⁸O = 18.5–20.6 ‰ in Alamas dolomitic marble (Table 3). Such results show that the dolomitic marble is a type of marine carbonate and partially melted (δ¹⁸O values decreased), which possibly involved with the hydrothermal fluids originating from granodiorite (Fig. 8).

3.4. SHRIMP oxygen isotope of zircons

According to previous research results, zircons in Alamas nephrite have the Th/U ratios of 0.05 ~ 0.39 (n = 13) (Fig. 9 A). The δ¹⁸O values of these zircons range from 5.69 to 8.85 ‰ (Fig. 2; Fig. 9B and C; Table 4, n = 25), slightly higher than the δ¹⁸O values of mantle magmatic zircons (5.3 ± 0.6 ‰, Valley et al., 1998; Page et al., 2007). Only one zircon has a large difference in δ¹⁸O value of 5.69 ‰ and 13.35 ‰ (Fig. 2D).

Zircons in Yurungkash & Karakash Rivers nephrite have the Th/U ratios of 0.03 ~ 2.39 (n = 24) (Fig. 9 A; Liu et al., 2016). The δ¹⁸O values of these zircons are 14.6 ~ 21.37 ‰ (Fig. 2; Fig. 9B and C; Table 4, n = 31), much higher than the δ¹⁸O values of mantle magmatic zircons. Only one zircon with age of 658.9 ± 8.9 Ma have Th/U ratio of 0.5 and δ¹⁸O value of 9.03 ± 0.08 ‰ (Table 4).

Table 2

Laser ablation-inductively coupled plasma-mass spectrometry (LA-ICP-MS) data of zircon trace element contents (ppm) in nephrite from Alamas and Yurungkash & Karakashgar Rivers deposits of Xinjiang, China.

Samples	QYZR-1-2	QYZR-1-6	QYZR-1-8	QYZR-1-21	QYZR-2-7	QYZR-2-15	QYZR-3-2	MYH-7-2	MYH-7-15	MYH-10-1	MYH-10-5	MYH-10-7	MYH-10-8	MYH-10-11	MYH-10-13	MYH-20-3	MYH-20-4
Y	8331	156	3332	238	861	1000	416	47.0	96.0	58.1	1765	280	373	138	316	232	123
La	0.15	0.02	0.02	0.08	0.00	0.00	0.09	0.00	0.02	0.00	0.01	0.00	0.96	0.01	0.02	0.04	0.00
Ce	20.6	0.45	27.8	1.93	5.92	3.42	3.84	0.11	0.26	0.08	0.29	0.07	11.2	0.25	0.73	1.27	0.32
Pr	0.10	0.02	0.11	0.06	0.01	0.01	0.02	0.00	0.01	0.00	0.02	0.00	1.07	0.00	0.00	0.01	0.00
Nd	1.86	0.22	3.15	0.51	0.18	0.17	0.32	0.07	0.10	0.09	0.09	0.04	10.1	0.07	0.21	0.25	0.06
Sm	7.03	0.00	7.30	0.32	0.71	0.59	0.50	0.06	0.18	0.06	0.09	0.07	4.74	0.14	0.40	0.17	0.12
Eu	2.52	0.02	2.26	0.17	0.26	0.24	0.19	0.02	0.07	0.03	0.05	0.00	2.19	0.10	0.11	0.13	0.16
Gd	62.7	0.48	37.4	1.70	5.40	6.84	3.08	0.56	1.04	0.23	2.33	0.71	8.59	1.59	4.10	2.29	1.25
Tb	24.6	0.30	11.6	0.65	2.22	2.62	1.03	0.11	0.35	0.17	1.74	0.39	2.25	0.50	1.40	0.84	0.49
Dy	438	5.79	188	10.4	38.9	46.6	18.4	2.46	5.64	3.25	53.4	10.5	30.9	8.86	21.4	14.5	9.10
Ho	170	2.86	64.1	4.03	16.0	18.6	7.50	0.85	1.93	1.21	30.7	4.58	9.88	2.90	6.61	5.55	3.21
Er	980	19.5	375	25.2	94.2	115	46.5	5.85	11.5	7.53	239	26.7	49.4	16.3	34.8	30.4	18.2
Tm	222	5.45	85.4	6.47	23.3	28.9	12.8	1.44	2.93	1.78	60.1	5.34	10.5	3.81	8.23	6.88	3.72
Yb	2309	70.7	963	74.8	281	335	176	15.9	33.2	23.0	664	55.7	112	41.3	91.1	79.7	40.5
Lu	379	14.5	168	15.6	50.1	68.1	40.6	2.64	5.05	3.58	81.1	9.53	13.4	6.01	11.9	10.2	5.54
Hf	10,401	13,418	5852	7183	9683	9321	4251	6643	8702	11,697	5879	6148	8567	11,431	17,270	6338	6580
Pb	19.9	0.51	51.6	1.90	5.72	3.27	5.77	2.31	3.56	0.89	7.30	0.39	6.81	4.51	13.1	10.9	4.69
Th	697	10.4	1649	57.3	187	117	189	74.0	104	23.2	254	11.6	199	139	414	342	157
U	2575	136	4461	146	696	579	666	183	246	33.0	4502	368	441	67.4	1101	379	188
Th/U	0.27	0.08	0.37	0.39	0.27	0.20	0.28	0.40	0.42	0.70	0.06	0.03	0.45	2.06	0.38	0.90	0.83
Nb/Ta	2.09	0.86	1.61	1.63	0.82	1.21	1.53	5.58	6.31	2.03	7.78	6.25	7.38	2.78	0.71	0.72	1.63
Yb/Sm	329	20,063	132	237	398	569	354	249	187	398	7724	752	23.6	297	228	456	336
Ce/Ce*	39.4	5.30	150	6.51	368	–	19.7	7.28	4.56	10.5	4.86	4.91	2.58	16.6	–	12.1	35.8
Eu/Eu*	0.37	1.30	0.42	0.72	0.41	0.37	0.46	0.33	0.49	0.87	0.32	0.03	1.05	0.68	0.25	0.62	1.28
(Sm/ La) _N	74.4	0.26	697	6.41	463	–	8.81	31.5	14.2	86.7	15.1	26.4	7.84	29.2	39.8	6.41	59.9
(Yb/ Gd) _N	45.5	183	31.8	54.4	64.1	60.4	70.3	35.3	39.5	124	351	97.4	16.1	32.0	27.4	42.9	40.1
ΣREY	12,949	276	5265	380	1379	1625	726	77	158	99	2898	393	640	219	498	384	205

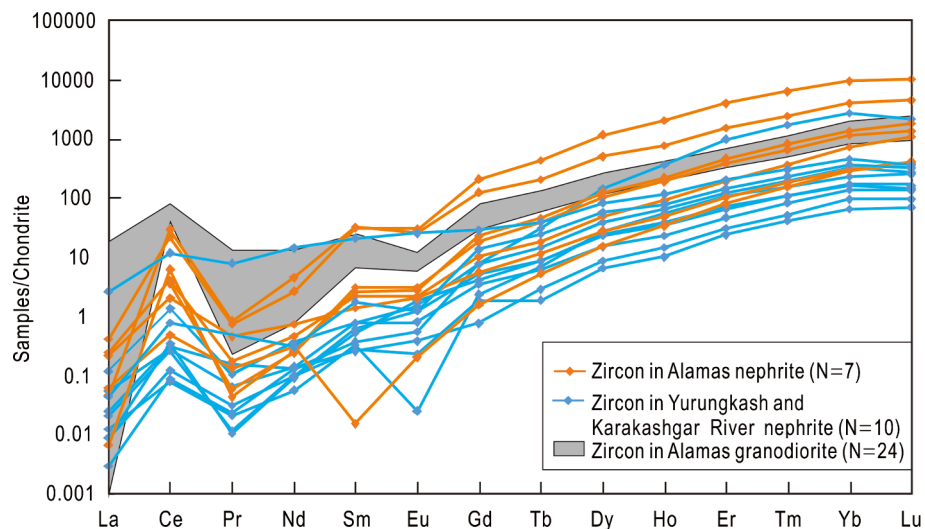


Fig. 6. Chondrite-normalized rare earth element (REE) patterns of zircons from Alamas and Yurungkash & Karakashgar Rivers nephrite deposits. Normalizing data are from Taylor and McLennan (1985).

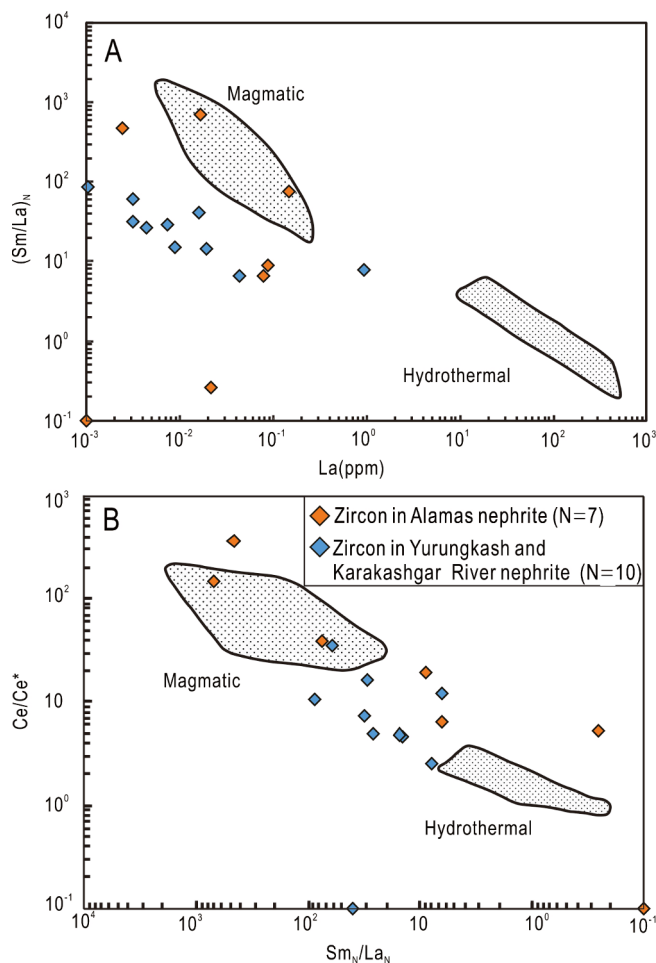


Fig. 7. Discrimination plots for magmatic and hydrothermal zircon (from Hoskin, 2005). (A) Chondrite-normalized Sm/La ratio vs La (ppm), and (B) Ce anomaly (Ce/Ce^*) vs $(Sm/La)_N$.

Table 3
C—O isotope compositions of dolomitic marble from Alamas nephrite deposit.

Sample	$\delta^{13}C_{C-V-PDB}\text{‰}$	$\delta^{18}O_{V-SMOW}\text{‰}$
ACa1	0.788	18.7
ACa2	0.979	19.8
ACa3	0.967	20.6
ACa4	0.896	19.5
ACa5	0.934	20.0
ACa6	0.987	19.9
ACa7	0.796	18.5
ACa8	1.024	20.6

4. Discussion

4.1. Comparison of granodiorite and Mg-skarn nephrite zircons

Zircon grains in the Alamas granodiorite are mainly euhedral, prismatic, colorless, with typical igneous oscillatory zoning, and contain small inclusions of albite, biotite, and feldspar (Zhang et al., 2016). All these zircons have Th/U ratios of 0.25–0.81 and a concordia age supporting a magmatic origin (Zhang et al., 2016). In contrast, zircons in Alamas nephrite are mainly subhedral and most have clear oscillatory zoning (Fig. 2). The Th/U values (0.05–0.39; Fig. 9A), a concordia ages (Liu et al., 2015), and REE patterns (i.e., obvious positive Ce anomalies and HREE enrichment) suggest that they are mainly magmatic zircons, similar to those in Alamas granodiorite, although some experienced hydrothermal alteration (Fig. 7).

The nephrite deposits along the Yurungkash & Karakashgar Rivers are placer deposits, sourced from the contact zone between the granodiorite and dolomitic marble (Liu et al., 2016). Zircons in nephrite have clear oscillatory zoning or obscure irregular zoning (Figure 3). The Th/U ratios (0.03–2.39; Fig. 9A), a concordia ages (Liu et al., 2016), and REE patterns (i.e., weak positive Ce anomalies and HREE enrichment) indicate they have a magmatic origin, although some zircons undergone hydrothermal alteration (Fig. 7).

4.2. Baddeleyite occurrence and formation in nephrite

The formation of skarn is a dynamic process that involves a magmatic stage, a contact metasomatic stage, and prograde and retrograde metasomatic stages, with each stage giving rise to a distinctive mineral assemblages in the contact zone (Meinert et al., 2005; Liu et al.,

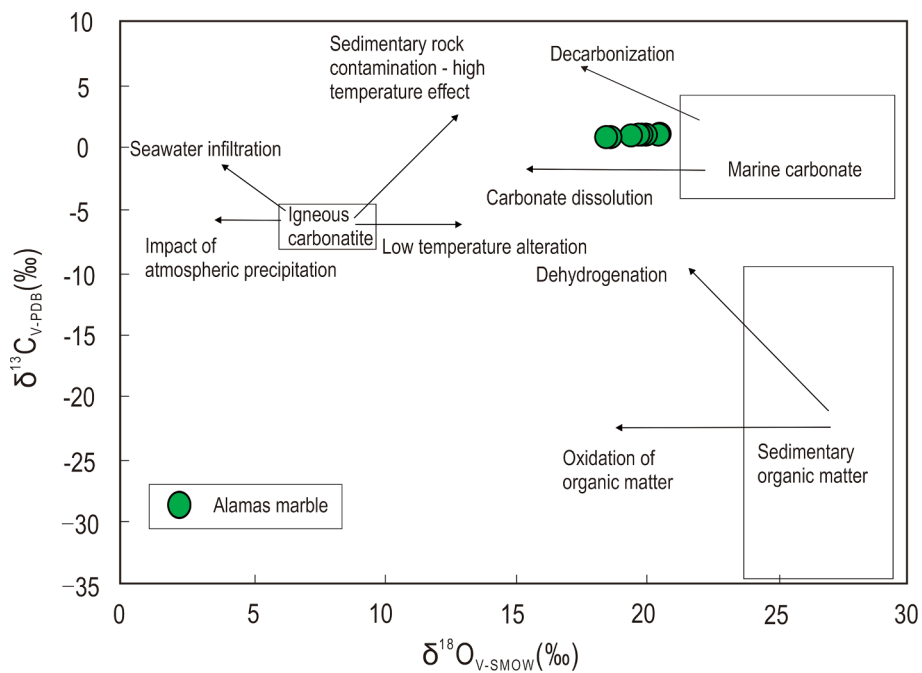
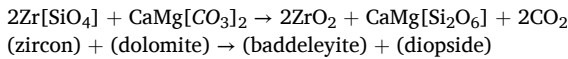


Fig. 8. C—O isotope values of the Alamas dolomitic marble.

2015, 2016). The baddeleyite grain in the nephrite occurs with apatite and has irregular strip-like shape rather than euhedral (Fig. 1C). It is assured baddeleyite have several occurrences. Firstly, baddeleyite can form during hydrothermal processes via the reaction of siliceous carbonates with enclosed zircon (Kato and Matsubara, 1991; Ferry, 1996a, b; Ferry et al., 2002; Fraser et al., 2004, Zhou et al., 2020). Secondly, baddeleyite can occur during the reaction between high field strength element (HFSE)-bearing fluids derives from surrounding magmas and carbonate rocks (Salvi and Williams-Jones, 1996; Migdisov et al., 2011; Zhao et al., 2016; Zhang et al., 2017). However, in this study, the formation of baddeleyite in nephrite formed through the reaction between zircon and dolomite. The zircon-to-baddeleyite reaction temperature is 660–710 °C at 3 kbar (Kato and Matsubara, 1991; Ferry, 1996a,b; Ferry et al., 2002), and the reaction is as follows:



The chemical instability of baddeleyite can result in grain edges being metasomatized by Si-rich magmatic fluids. The above reaction did not continue until completion, so remnant baddeleyite occurs in zircon (Fig. 4).

4.3. Zircon oxygen isotope in nephrite can be affected by oxygen isotope in dolomitic marble

Based on the geological setting, petrographic characteristics (Figs. 2 and 3), U–Pb ages (Fig. 9A and B), and major and trace element geochemistry (Figs. 5–7), zircons in nephrite are mainly igneous in origin. The δ¹⁸O values of the Alamas nephrite zircons range from 5.69 ‰ to 8.85 ‰ with an exception of 13.35 ‰ (Table 4; Fig. 9C), which close to the values of zircons in the Alamas granodiorite (δ¹⁸O_{zircon} = 6.4 ‰–9.0 ‰; Fig. 9D; Zhang et al., 2016) but slightly higher than the values of magmatic zircons from the mantle (5.3 ‰ ± 0.6 ‰; Valley et al., 1998; Page et al., 2007).

Zircons in Yurungkash & Karakash Rivers nephrite yield δ¹⁸O values of 14.6 ‰ to 21.37 ‰ with an exception of 9.03 ‰ (Table 4; Fig. 9C), which are higher than those of Alamas nephrite zircons. External fluids interacting with pre-existing igneous zircons would not raise the δ¹⁸O values up to >15 ‰; such a change would require processes such as dissolution/reprecipitation or recrystallization, but these processes are

inconsistent with the petrographic characteristics of zircons in nephrite (Figs. 2 and 3). Therefore, we infer that these high-δ¹⁸O zircons crystallized from high-δ¹⁸O magma, and do not reflect post-magmatic alteration. Besides, the δ¹⁸O values of marine carbonate rocks can be as high as 25 ‰ (Valley et al., 2005). A small amount of marine carbonate rock assimilated into melt could lead to the significant δ¹⁸O in magma and zircons. The granodiorite experienced partial exchange of δ¹⁸O with the Alamas dolomitic marble (δ¹³C = 0.79 ‰–1.02 ‰, δ¹⁸O = 18.5 ‰–20.6 ‰) during the upwelling of granodiorite. Thus, the high δ¹⁸O nephrite zircons may have initially formed as high δ¹⁸O grains within endoskarn, which occurred along but within the margin of the granitoid where marble was assimilated into the melt. In this scenario, the zircons can have preserved igneous growth zoning, and the high δ¹⁸O is attributed to crystallization as a magmatic phase from a high δ¹⁸O reservoir (granitoid magma contaminated with marble along the margin/skarn). Then, owing to the addition of meteoric water and volatile matter removal, the δ¹⁸O values of most tremolite (0.8 ‰–7.9 ‰) are lower than dolomitic marble (18.7 ‰–20.6 ‰) and granodiorite (4.6 ‰–8.7 ‰).

5. Conclusions

1. Based on the geological setting, petrographic characteristics, U–Pb ages, and major and trace element characteristics, most zircons in nephrite from Alamas and Yurungkash & Karakash Rivers deposits are mainly igneous in origin.

2. Baddeleyite inclusions are irregular, fragmented, or granular, and occur within zircons or in fissures of zircons in nephrite. Such petrographic characteristics suggest that the baddeleyite formed during the following reaction between zircon and dolomite at 3 kbar and 660–710 °C: $2\text{Zr}[\text{SiO}_4] + \text{CaMg}[\text{CO}_3]_2 \rightarrow 2\text{ZrO}_2 + \text{CaMg}[\text{Si}_2\text{O}_6] + 2\text{CO}_2$.

3. The Alamas dolomitic marble has δ¹³C = 0.79 ‰–1.02 ‰ and δ¹⁸O = 18.7 ‰–20.6 ‰, suggesting it is the product of partial dissolution of marine carbonate during contact metasomatism with granodiorite.

4. Predominant zircons in the Alamas nephrite have δ¹⁸O values of 5.69 ‰–8.85 ‰ (n = 25), close to the values of zircons in the granodiorite (6.4 ‰–9.0 ‰). Most zircon δ¹⁸O values range from 14.6 ‰ to 21.37 ‰ in Yurungkash & Karakash Rivers nephrite. A more likely scenario is that the high δ¹⁸O zircons in nephrite may have initially formed as high δ¹⁸O grains within endoskarn, which occurred along but

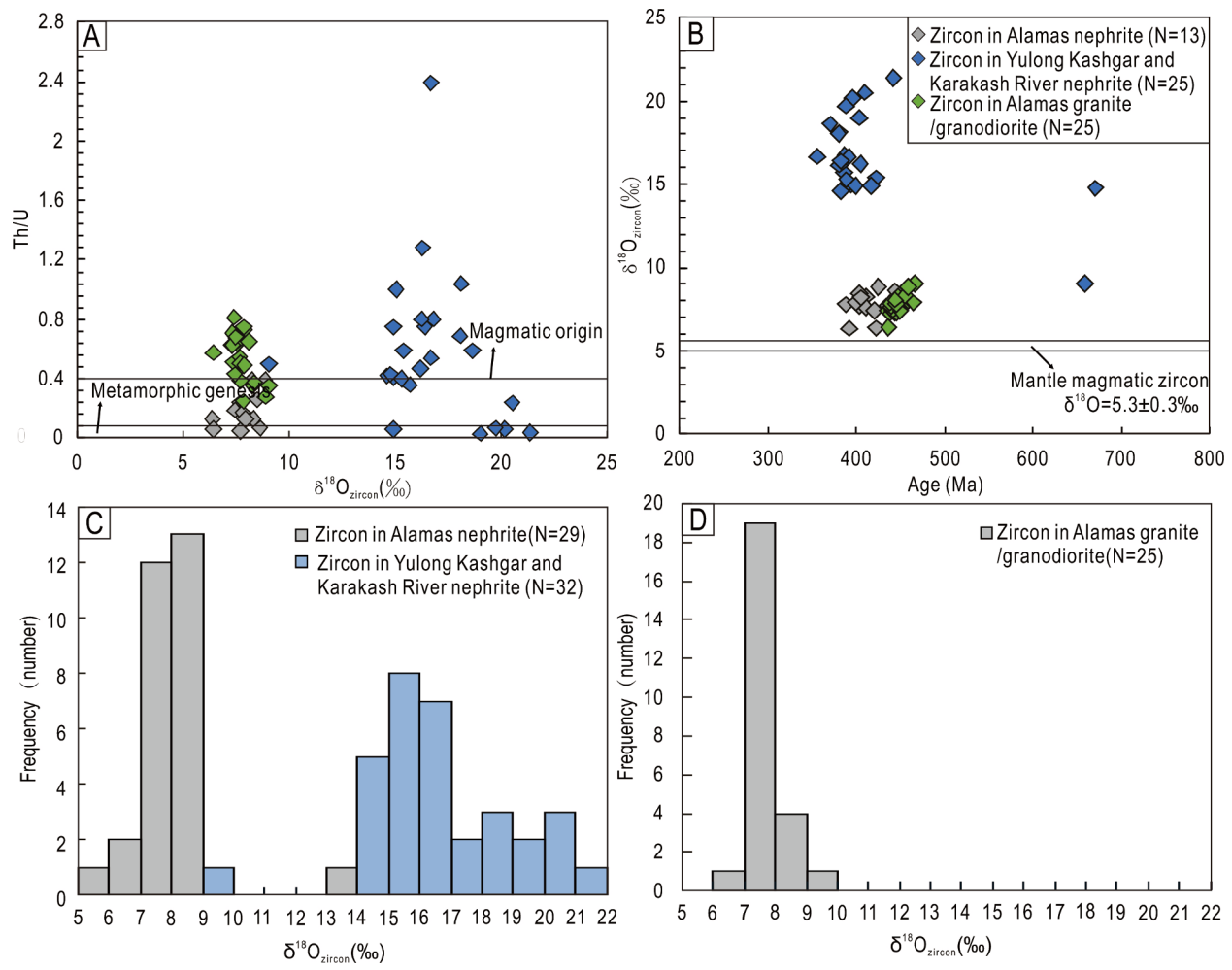


Fig. 9. Zircon $\delta^{18}\text{O}$ ($\delta^{18}\text{O}_{\text{zircon}}$) vs (A) Th/U and (B) age for Alamas and Yurungkash & Karakash Rivers nephrite and granodiorite (age data from Liu et al., 2015, 2016; Zhang et al., 2016; $\delta^{18}\text{O}_{\text{zircon}}$ data from the present study). (C) Histograms of $\delta^{18}\text{O}_{\text{zircon}}$ values in nephrite samples (this study). (D) Histograms of $\delta^{18}\text{O}_{\text{zircon}}$ values from Alamas granodiorite (data from Zhang et al., 2016).

Table 4

Sensitive high-resolution ion microprobe (SHRIMP) data of zircon oxygen isotope compositions in nephrite and granodiorite from Alamasand Yurungkash & Karakashgar Rivers deposits of Xinjiang, China.

Sample	mineral	Th/U	$^{206}\text{Pb}/^{238}\text{U}$ age (Ma)	$\delta^{18}\text{O}$ (‰)	Error (‰)
Alamas nephrite deposit					
AHg13-1	Zircon in granodiorite	0.69	448.5 ± 6.5	7.54	0.34
AHg13-2	Zircon in granodiorite	0.25	444.1 ± 6.4	7.80	0.36
AHg13-3	Zircon in granodiorite	0.51	437.1 ± 6.4	7.47	0.27
AHg13-4	Zircon in granodiorite	0.39	451.7 ± 6.6	7.67	0.29
AHg13-5	Zircon in granodiorite	0.35	466.3 ± 6.8	9.03	0.34
AHg13-6	Zircon in granodiorite	0.63	448.7 ± 6.5	7.55	0.32
AHg13-7	Zircon in granodiorite	0.67	448.6 ± 6.5	7.48	0.29
AHg13-8	Zircon in granodiorite	0.35	447.0 ± 6.5	8.25	0.31
AHg13-9	Zircon in granodiorite	0.81	435.6 ± 6.4	7.39	0.28
AHg13-10	Zircon in granodiorite	0.64	447.9 ± 6.5	7.43	0.19
AHg13-11	Zircon in granodiorite	0.63	438.5 ± 6.9	7.25	0.31
AHg13-12	Zircon in granodiorite	0.51	442.0 ± 6.4	7.35	0.28
AHg13-13	Zircon in granodiorite	0.57	436.4 ± 6.4	6.40	0.29
AHg13-14	Zircon in granodiorite	0.71	444.0 ± 6.5	7.29	0.33
AHg13-15	Zircon in granodiorite	0.63	445.2 ± 6.5	7.29	0.34
AHg13-16	Zircon in granodiorite	0.68	441.3 ± 6.5	7.47	0.3
AHg13-17	Zircon in granodiorite	0.38	455.2 ± 6.6	8.34	0.31
AHg13-18	Zircon in granodiorite	0.73	464.7 ± 6.7	7.89	0.33
AHg13-19	Zircon in granodiorite	0.54	438.3 ± 6.4	7.64	0.28
AHg13-20	Zircon in granodiorite	0.51	438.7 ± 6.4	7.66	0.31
AHg13-21	Zircon in granodiorite	0.43	449.8 ± 6.5	7.40	0.17
AHg13-22	Zircon in granodiorite	0.49	438.1 ± 6.4	7.86	0.38
AHg13-23	Zircon in granodiorite	0.28	458.3 ± 6.6	8.86	0.24
AHg13-24	Zircon in granodiorite	0.75	445.1 ± 6.5	7.84	0.18
AHg13-25	Zircon in granodiorite	0.65	443.9 ± 6.4	8.07	0.26
QYZR1-02	Zircon in nephrite	0.13	392.0 ± 4.9	6.36	0.13
QYZR1-03	Zircon in nephrite	0.39	424.6 ± 6.2	8.83	0.12
QYZR1-04	Zircon in nephrite	0.24	403.4 ± 5.2	7.68	0.12
QYZR1-05	Zircon in nephrite			8.55	0.12
QYZR1-06	Zircon in nephrite			7.42	0.16
QYZR1-07	Zircon in nephrite			8.85	0.16
QYZR1-08	Zircon in nephrite			8.51	0.14
QYZR1-09	Zircon in nephrite			7.97	0.09
QYZR1-10	Zircon in nephrite			7.73	0.13
QYZR1-11	Zircon in nephrite			8.43	0.10
QYZR1-12	Zircon in nephrite			8.12	0.07
QYZR1-19	Zircon in nephrite			8.61	0.11
QYZR1-21	Zircon in nephrite			7.60	0.10
QYZR1-24	Zircon in nephrite	0.06	422.3 ± 6.6	6.39	0.08
QYZR1-25	Zircon in nephrite			8.29	0.09
QYZR1-32	Zircon in nephrite	0.13	411.6 ± 5.3	8.27	0.07
QYZR2-01	Zircon in nephrite	0.17	410.3 ± 6.1	7.61	0.07
QYZR2-03	Zircon in nephrite			7.62	0.14
QYZR2-05	Zircon in nephrite	0.19	420.3 ± 6.8	7.41	0.10
QYZR2-07	Zircon in nephrite			8.07	0.13
QYZR2-09	Zircon in nephrite	0.17	388.1 ± 6.0	7.79	0.15
QYZR2-10	Zircon in nephrite			13.35	0.38
QYZR2-11	Zircon in nephrite			5.69	0.21
QYZR2-13	Zircon in nephrite	0.05	434.3 ± 7.5	7.68	0.13
QYZR2-15	Zircon in nephrite	0.13	399.2 ± 5.9	7.90	0.11
QYZR2-16	Zircon in nephrite	0.26	403.3 ± 6.4	8.47	0.25
QYZR2-20	Zircon in nephrite	0.07	443.9 ± 8.4	8.60	0.18
QYZR2-21	Zircon in nephrite	0.39	405.3 ± 6.2	8.19	0.16
QYZR3-2	Zircon in nephrite			7.90	0.12
Yurungkash and Karakashgar Rivers placer nephrite deposit					
MYH-7-1	Zircon in nephrite	1.28	384.1 ± 6.2	16.29	0.21
MYH-7-2	Zircon in nephrite	0.80	386.7 ± 6.2	16.77	0.18
MYH-7-3	Zircon in nephrite	2.39	355.3 ± 8.5	16.67	0.16
MYH-7-4	Zircon in nephrite	0.41	393.0 ± 7.0	14.93	0.33
MYH-7-5	Zircon in nephrite	0.36	386.1 ± 6.3	15.67	0.13
MYH-7-6	Zircon in nephrite	0.54	391.4 ± 8.8	16.67	0.15
MYH-7-7	Zircon in nephrite	0.42	382.0 ± 6.9	14.60	0.23
MYH-7-8	Zircon in nephrite	0.47	380.5 ± 5.7	16.17	0.27
MYH-7-9	Zircon in nephrite			15.78	0.16
MYH-7-10	Zircon in nephrite			15.17	0.21
MYH-7-13	Zircon in nephrite			15.60	0.22
MYH-7-15	Zircon in nephrite			15.41	0.18
MYH-20-1	Zircon in nephrite	0.59	370.0 ± 6.3	18.62	0.14
MYH-20-2	Zircon in nephrite	1.04	380.8 ± 6.2	18.11	0.15
MYH-20-3	Zircon in nephrite			17.63	0.18
MYH-20-4	Zircon in nephrite	0.69	379.5 ± 6.2	18.04	0.13
MYH-20-6	Zircon in nephrite			17.52	0.16

(continued on next page)

Table 4 (continued)

Sample	mineral	Th/U	$^{206}\text{Pb}/^{238}\text{U}$ age (Ma)	$\delta^{18}\text{O}$ (‰)	Error (‰)
MYH-10-01	Zircon in nephrite	0.75	382.3 ± 9.3	16.38	0.11
MYH-10-02	Zircon in nephrite	0.59	422.5 ± 5.8	15.38	0.08
MYH-10-03	Zircon in nephrite	0.06	395.4 ± 4.8	20.18	0.10
MYH-10-04	Zircon in nephrite	1.00	391.3 ± 4.7	15.03	0.08
MYH-10-05	Zircon in nephrite	0.06	398.6 ± 4.7	14.89	4.27
MYH-10-06	Zircon in nephrite	0.03	403.2 ± 4.9	19.00	3.89
MYH-10-07	Zircon in nephrite	0.07	387.8 ± 4.6	19.71	0.10
MYH-10-08	Zircon in nephrite	0.40	388.4 ± 4.9	15.27	0.09
MYH-10-10	Zircon in nephrite	0.75	416.8 ± 5.3	14.90	0.16
MYH-10-11	Zircon in nephrite	0.80	404.6 ± 6.8	16.22	0.10
MYH-10-12	Zircon in nephrite	0.04	442.0 ± 5.9	21.37	0.09
MYH-10-13	Zircon in nephrite	0.24	409.7 ± 4.9	20.52	0.13
MYH-10-09	Zircon in nephrite	0.43	670.8 ± 8.4	14.76	0.06
MYH-10-14	Zircon in nephrite	0.50	658.9 ± 8.9	9.03	0.08
MYH-10-15	Zircon in nephrite			20.22	0.12

Zircon age dates in nephrite from Liu et al., 2015, 2016; Zircon age and oxygen isotope dates in granodiorite from Zhang et al., 2016.

within the margin of the granitoid where marble was assimilated into the melt.

Declaration of Competing Interest

The authors declare that they have no known competing financial interests or personal relationships that could have appeared to influence the work reported in this paper.

Data availability

Data will be made available on request.

Acknowledgments

This research was funded by the Strategic Priority Research Program of the Chinese Academy of Sciences (Grant No. XDA20070304); Second Tibetan Plateau Scientific Expedition and Research (Grant No. 2021QZKK0304); the Key Special Project for Introduced Talents Team of Southern Marine Science and Engineering, Guangdong Laboratory, Guangzhou (Grant No. GML2019ZD0106); the National Natural Science Foundation of China (Grant Nos 92162216, 41922014); and the China Geological Survey Program of the China Geological Survey, Ministry of Natural Resources (Grant No. DD 20221649). We are grateful to the reviewers, who provided constructive suggestions that helped to improve the manuscript.

Appendix A. Supplementary data

Supplementary data to this article can be found online at <https://doi.org/10.1016/j.oregeorev.2022.105087>.

References

- Bindeman, I.N., Valley, J.W., 2000. Formation of low- $\delta^{18}\text{O}$ rhyolites after caldera collapse at Yellowstone, Wyoming, USA. *Geology* 28 (8), 719–722.
- Bindeman, I.N., Valley, J.W., 2001. Low- $\delta^{18}\text{O}$ rhyolites from Yellowstone: magmatic evolution based on analyses of zircons and individual phenocrysts. *J. Petrol.* 42 (8), 1491–1517.
- Cavosie, A.J., Valley, J.W., Kita, N.T., et al., 2011. The origin of high $\delta^{18}\text{O}$ zircons: marbles, megacrysts, and metamorphism. *Contrib. Miner. Petrol.* 162, 961.
- Claesson, S., Bibikova, E.V., Shumlyansky, L., et al., 2016. Can oxygen isotopes in magmatic zircon be modified by metamorphism? A case study from the Eoarchean Dniester-Bug Series, Ukrainian Shield. *Precambr. Res.* 273, 1–11.
- Deng, J., Wang, Q.F., Li, G.J., Li, C.S., Wang, C.M., 2013. Tethys tectonic evolution and its bearing on the distribution of important mineral deposits in the Sanjiang region, SW China. *Gondwana Res.* 26 (2), 419–437.
- Deng, J., Wang, Q.F., Li, G.J., Santosh, M., 2014. Cenozoic tectono-magmatic and metallogenic processes in the Sanjiang region, southwestern China. *Earth-Sci. Rev.* 138, 268–299.
- Eiler, J.M., 2001. Oxygen isotope variations of basaltic lavas and upper mantle rocks. *Rev. Mineral. Geochem.* 43 (1), 319–364.
- Einaudi, M.T., Meinert, L.D., Newberry, R.J., 1981. Skarn deposits. *Econ. Geol.* 75, 317–391.
- Ferry, J.M., 1996a. Three novel isograds in metamorphosed siliceous dolomites from the Ballachulish aureole, Scotland. *Am. Miner.* 81, 485–494.
- Ferry, J.M., 1996b. Prograde and retrograde fluid flow during contact metamorphism of siliceous carbonate rocks from the Ballachulish aureole, Scotland. *Contrib. Miner. Petrol.* 124, 235–254.
- Ferry, J.M., Newton, R.C., Manning, C.E., 2002. Experimental determination of the equilibria: rutile + magnesite = geikielite + CO_2 and zircon + 2magnesite = baddeleyite + forsterite + 2CO_2 . *Am. Miner.* 87, 1342–1350.
- Fraser, G.L., Pattison, D.R.M., Heaman, L.M., 2004. Age of the Ballachulish and Glencoe Igneous Complexes (Scottish Highlands), and paragenesis of zircon, monazite and baddeleyite in the Ballachulish Aureole. *Geolog. Soc.* 161, 447–462.
- Gao, J., Reiner, K., 2000. Eclogite occurrences in the southern Tianshan high pressure belt, Xinjiang, Western China. *Gondwana Res.* 3, 33–38.
- Grimes, C.B., Ushikubo, T., Kozdon, R., et al., 2013. Perspectives on the origin of plagiogranite in ophiolites from oxygen isotopes in zircon. *Lithos* 179, 48–66.
- Harlow, G.E., Sorensen, A.S.S., 2001. Jade: occurrence and metasomatic origin. *The Australian Gemmologist* 21, 7–10.
- Harlow, G.E., Sorensen, A.S.S., 2005. Jade (nephrite and jadeite) and serpentinite: Metasomatic connections. *Int. Geol. Rev.* 47 (2), 113–146.
- Hoskin, P.W.O., 2003. The Composition of Zircon and Igneous and Metamorphic Petrogenesis. *Rev. Mineral. Geochem.* 53 (1), 27–62. <https://doi.org/10.2113/0530027>.
- Hoskin, P.W.O., 2005. Trace-element composition of hydrothermal zircon and the alteration of Hadean zircon from the Jack Hills, Australia. *Geochim. Cosmochim. Acta* 69 (3), 637–648.
- Jiang, R.H., 1986. Preliminary study on genetic type, minerogenetic model and the law of distribution of Hotan nephrite. *Xinjiang Geol.* 4, 1–12 in Chinese.
- Kato, A., Matsubara, S., 1991. Geikielite, baddeleyite and zirconolite in dolomitic marble from the Neichi mine, Miyako City, Iwate Prefecture, Japan. *Bull. National Sci. Museum* 17, 11–20.
- Leaming, S.F., 1978. Jade in Canada. *Geological Survey of Canada Papers Press*, Ottawa, pp. 1–59.
- Liu, Y., Deng, J., Shi, G.H., et al., 2010. Chemical zone of nephrite in Alamas, Xinjiang, China. *Resour. Geol.* 60 (3), 249–259.
- Liu, Y., Deng, J., Shi, G.H., et al., 2011. Geochemistry and petrology of nephrite from Alamas, Xinjiang, NW China. *J. Asian Earth Sci.* 42, 440–451.
- Liu, Y., Zhang, R.Q., Zhang, Z.Y., Shi, G.H., Abuduwayiti, M., Liu, J.H., 2015. Mineral inclusions and SHRIMP U-Pb dating of zircons from the Alamas nephrite and granodiorite: implications for the genesis of a magnesian skarn deposit. *Lithos* 212–215, 128–144.
- Liu, Y., Zhang, R.Q., Abuduwayiti, M., et al., 2016. SHRIMP U-Pb zircon ages, mineral compositions and geochemistry of placer nephrite in the Yurungkash and Karakash River deposits, West Kunlun, Xinjiang, northwest China: implication for a magnesium skarn. *Ore Geol. Rev.* 72, 699–727.
- Mao, J.W., Goldfarb, R.J., Wang, Y.T., Hart, C.J., Yang, J.M., Wang, Z.L., 2005. Late Paleozoic base and precious metal deposits, East Tianshan, Xinjiang, China: characteristics and geodynamic setting. *Episodes* 28 (1), 23–36.
- Meinert, L., Dipple, G., Nicolescu, S., 2005. World skarn deposits. *Econ. Geol.* 100, 299–336.
- Migdisov, A.A., Williams-Jones, A.E., van Hinsberg, V., et al., 2011. An experimental study of the solubility of baddeleyite (ZrO_2) in fluoride-bearing solutions at elevated temperature. *Geochim. Cosmochim. Acta* 75, 7426–7434.
- Monani, S., Valley, J.W., 2001. Oxygen isotope ratios of zircon: magma genesis of low $\delta^{18}\text{O}$ granites from the British Tertiary igneous province, western Scotland. *Earth Planet. Sci. Lett.* 184 (2), 377–392.
- Page, F.Z., Ushikubo, T., Kita, N.Y., et al., 2007. High-precision oxygen isotope analysis of picogram samples reveals 2 μm gradients and slow diffusion in zircon. *Am. Mineral.* 92 (10), 1772–1775.
- Peck, W.H., Valley, J.W., Wilde, S.A., et al., 2001. Oxygen Isotope ratios and rare earth elements in 3. 3 to 4. 4 Ga zircons: Ion microprobe evidence for high $\delta^{18}\text{O}$

- continental crust and oceans in the Early Archean. *Geochim. Cosmochim. Acta* 65 (22), 4215–4229.
- Roberts, N.M.W., Santosh, M., 2018. Capturing the Mesoarchean emergence of continental crust in the Coorg Block, southern India. *Geophys. Res. Lett.* 45, 7444–7453.
- Rubenach, M., Structural controls of metasomatism on a regional scale. In D.E. Harlov and A. Häkon, Eds., *Metasomatism and the Chemical Transformation of Rock*, 2013: 93–140.
- Salvi, S., Williams-Jones, A.E., 1996. The role of hydrothermal processes in concentrating high-field strength elements in the Strange Lake peralkaline complex, northeastern Canada. *Geochim. Cosmochim. Acta* 60, 1917–1932.
- Spencer, C.J., Cavosie, A.J., Raub, T.D., et al., 2017. Evidence for melting mud in Earth's mantle from extreme oxygen isotope signatures in zircon. *Geology* 45, 975–978.
- Spencer, C.J., Cavosie, A.J., Morrell, T.R., et al., 2022. Disparities in oxygen isotopes of detrital and igneous zircon identify erosional bias in crustal rock record. *Earth Planet. Sci. Lett.* 577, 117248.
- Tang, Y.L., Chen, B.Z., Jiang, R.H., 1994. Chinese Hetian nephrite, Xinjiang: Xinjiang People's Publishing House, p. 103–206. (in Chinese with English abstract).
- Taylor, S.R., McLennan, S.M., 1985. The continental crust: its composition and evolution. *J. Geol.* 94 (4), 57–72.
- Taylor, H.P., Oxygen and hydrogen isotope relationships in hydrothermal mineral deposits. *Geochemistry of Hydrothermal Ore Deposits*, 1997: 229–302. Taylor Jr HP. The oxygen isotope geochemistry of igneous rocks. Contributions to Mineralogy and Petrology, 1968, 19(1): 1–71.
- Valley, J.W., Chiarenzelli, J.R., McLelland, J.M., 1994. Oxygen isotope geochemistry of zircon. *Earth Planet. Sci. Lett.* 126 (4), 187–206.
- Valley, J.W., Kiny, P.D., Schulze, D.J., et al., 1998. Zircon megacrysts from kimberlite: oxygen isotope variability among mantle melts. *Contrib. Miner. Petrol.* 133 (1–2), 1–11.
- Valley, J.W., Lackey, J.S., Cavosie, A.J., et al., 2005. 4.4 billion years of crustal maturation: oxygen isotope ratios of magmatic zircon. *Contrib. Miner. Petrol.* 150, 561–580.
- Wang, Z.Q., Jiang, C.F., Yan, Q.R., Yan, Z., 2001. Accretion and collision orogenes in the West Kunlun Mountains, China. *Gondwana Res.* 4, 843–844.
- Wei, C.S., Zhao, Z.F., Spicuzza, M.J., 2008. Zircon oxygen isotopic constraint on the sources of Late Mesozoic A-type granites in eastern China. *Chem. Geol.* 250 (1–4), 1–15.
- Xiao, W.J., Windley, B.F., Fang, A.M., Yuan, C., Wang, Z.H., Hao, J., Hou, Q.L., 2001. Palaeozoic-Early Mesozoic accretionary tectonics of the Western Kunlun Range. NW China. *Gondwana Res.* 4, 826–827.
- Xiao, W.J., Windley, B.F., Liu, D.Y., Jian, P., Liu, C.Z., Yuan, C., Sun, M., 2005. Accretionary tectonics of the Western Kunlun Orogen, China: a Paleozoic-Early Mesozoic, long-lived active continental margin with implications for the growth of Southern Eurasia. *J. Geol.* 113, 687–705.
- Yang, S., Li, Z.L., Chen, H.L., Santosh, M., Dong, C.W., Yu, X., 2007. Permian bimodal dyke of Tarim Basin; NW China: Geochemical characteristics and tectonic implications. *Gondwana Res.* 12, 113–120.
- Yui, T.F., Kwon, S.T., 2002. Origin of a dolomite-related jade deposit at Chuncheon, Korea. *Econ. Geol.* 97, 593–601.
- Zhang, Q.C., Liu, Y., Huang, H., et al., 2016. Petrogenesis and tectonic implications of the high-K Alamas calc-alkaline granitoids at the northwestern margin of the Tibetan Plateau: Geochemical and Sr-Nd-Hf-O isotope constraints. *J. Asian Earth Sci.* 127, 137–151.
- Zhang, S.H., Zhao, Y., Li, Q.L., et al., 2017. First identification of baddeleyite related/linked to contact metamorphism from carbonatites in the world's largest REE deposit, Bayan Obo in North China Craton. *Lithos* 284–285, 654–665.
- Zhao, W.W., Zhou, M.F., Chen, W.T., 2016. Growth of hydrothermal baddeleyite and zircon in different stages of skarnization. *Am. Miner.* 101, 2689–2700.
- Zheng, Y.F., Fu, B., Gong, B., et al., 1998. Carbon isotope anomaly in marbles associated with eclogites from the Dabie Mountains. *Chin. Sci. Bull.* 43, 155–160.
- Zhou, G.Y., Wu, Y.B., Fu, B., et al., 2020. Genesis of baddeleyite and high $\delta^{18}\text{O}$ zircon in impure marble from the Tongbai orogen, Central China: insights from petrochronology and Hf-O isotope compositions. *Contrib. Miner. Petrol.* 175, 75.